Metal-Bridged Graphene–Protein Supraparticles for Analog and Digital Nitric Oxide Sensing

Zhi-Bei Qu, Xinguang Zhou, Min Zhang, Jianlei Shen, Qian Li, Feng Xu,* Nicholas Kotov,* and Chunhai Fan*

Self-limited nanoassemblies, such as supraparticles (SPs), can be made from virtually any nanoscale components, but SPs from nanocarbons including graphene quantum dots (GQDs), are hardly known because of the weak van der Waals attraction between them. Here it is shown that highly uniform SPs from GQDs can be successfully assembled when the components are bridged by Tb^{3+} ions supplementing van der Waals interactions. Furthermore, they can be coassembled with superoxide dismutase, which also has weak attraction to GQDs. Tight structural integration of multilevel components into SPs enables efficient transfer of excitonic energy from GQDs and protein to Tb^{3+}. This mechanism is activated when Cu^{2+} is reduced to Cu^{1+} by nitric oxide (NO)—an important biomarker for viral pulmonary infections and Alzheimer's disease. Due to multipronged fluorescence enhancement, the limit of NO detection improves 200 times reaching 10×10^{-12} M. Furthermore, the uniform size of SPs enables digitization of the NO detection using the single particle detection format resulting in confident registration of as few as 600 molecules mL^{-1}. The practicality of the SP-based assay is demonstrated by the successful monitoring of NO in human breath. The biocompatible SPs combining proteins, carbonaceous nanostructures, and ionic components provide a general path for engineering uniquely sensitive assays for noninvasive tracking of infections and other diseases.

1. Introduction

Mesoscale superstructures from nanoscale components displaying self-limited growth represent a rapidly expanding family of nanoassemblies. Their signature is the emergence of monodispersed meso- and microscale particles[1–3] and fibers[4,5] from polydispersed heterogeneous components. Self-limited growth leads to quasi-equilibrium states where repulsive and attractive interactions between the components compensate each other and restrict the assembly dimensions to a particular size. Despite the synthetic simplicity of this approach, exceptionally complex structures can be produced following the self-limited mechanism when the competition of several restrictions takes place.[6,7]

Besides layer-by-layer-assembled films, one of the most representative members of self-limited nanoassemblies is supraparticles (SPs) incorporating 100–300 constitutive nanoscale units whose formation is governed by the balance between electrostatic repulsions and van der Waals (vdW) attractions.[3,8] The versatility of SP components, sub-nanoscale porosity, and ability to incorporate biological subunits stimulated studies of self-limited SPs toward protein stabilization,[9] drug delivery,[10] photocatalysis,[11] chiral recognition,[12] and chiral catalysis.[2,13]

Many inorganic nanoparticles (NPs) readily produce SPs, however, carbonaceous nanoscale components[14] such as graphene NPs, do not.[15] The reason is partially from that their

Dr. Z.-B. Qu, Prof. F. Xu
Joint Research Center for Precision Medicine
Shanghai Jiao Tong University Affiliated Sixth People's Hospital
South Campus
Southern Medical University Affiliated Fengxian Hospital
Shanghai 201499, China
E-mail: xuf@smu.edu.cn

Dr. Z.-B. Qu, Dr. J. Shen, Prof. Q. Li, Prof. C. Fan
School of Chemistry and Chemical Engineering and Frontiers Science
Center for Transformative Molecules
Shanghai Jiao Tong University
Shanghai 200241, China
E-mail: fanchunhai@sjtu.edu.cn

Dr. X. Zhou
Shenzhen NTEK Testing Technology Co., Ltd.
Building E in Fenda Science Park, Baoan District, Shenzhen 518000, China

The ORCID identification number(s) for the author(s) of this article
can be found under https://doi.org/10.1002/adma.202007900.

Dr. X. Zhou, Prof. M. Zhang
School of Chemistry and Molecular Engineering
East China Normal University
Shanghai 200241, China

Prof. N. Kotov
Department of Chemical Engineering, Department of Materials Science
and Engineering, Department of Biomedical Engineering
Biointerfaces Institute
University of Michigan
Ann Arbor, MI 48109, USA
E-mail: kotov@umich.edu

Prof. C. Fan
Institute of Molecular Medicine
Shanghai Key Laboratory for Nucleic Acids Chemistry
and Nanomedicine
Renji Hospital
School of Medicine
Shanghai Jiao Tong University
Shanghai 200127, China

**ADVANCED
SCIENCE NEWS**

www.advancedsciencenews.com

**ADVANCED
MATERIALS**

www.advmat.de

vdW attractions are relatively weaker than the dispersive forces for metallic, semiconductor, and ceramic NPs owing to the small atomic mass of carbon. At the same time, the unique optical, electronic, biological, and mechanical properties of nanocarbons are needed in many nanoassemblies being translated to practice. Graphene fragments smaller than 100 nm, also known as graphene quantum dots (GQDs),[16–22] would be nearly ideal components for SPs because of their simplicity of syntheses, high relative earth abundance, strong optical activity, and biological compatibility.[23,24] While GQDs can form some nanoassemblies,[4,25] the challenge for their successful self-organization into monodispersed SPs is the mediation of sufficient and simultaneous repulsion and attraction.

In this work, highly uniform SPs were assembled from GQDs and superoxide dismutase (SOD), when attractive vdW forces were enhanced by coordination interactions with terbium ions (Tb^{3+}). Tight structural integration of optically active components into SPs makes possible efficient energy transfer between the protein and GQD to the Tb^{3+} fluorophore. SOD protein is an enzyme that alternately catalyzes the dismutation of the superoxide (O_2^-) radicals, usually consisting of copper and zinc as active centers. Being augmented by stimulated intersystem crossing, when Cu (II) in SOD is reduced to Cu (I), the multipronged fluorescence enhancement of Tb^{3+} engenders highly selective detection of small molecules that have penetrated. This new capability of self-limited nanoassemblies was demonstrated for sensing nitric oxide (NO)—an essential marker for many metabolic processes[26] and cellular signaling.[27] Its continuous monitoring is essential for the treatment of coronary heart health,[28] Alzheimer's disease,[29] and psychiatric disorders.[30] The presence of NO in human breath can also serve as the basis for a rapid test for pulmonary infections,[31] including severe acute respiratory syndrome (SARS)[32,33] and COVID-19.[34] We found that GQD-based SPs enable highly sensitive NO probes, which is an improvement of current methods by at least two orders of magnitude. SPs assembled from GQD, Tb^{3+}, and SOD also display high selectivity for NO over other reactive nitrogen (RNS) and oxygen species (ROS). Furthermore, the convenient size and uniformity of SPs combined with strong luminesce enable NO detection via single-particle counting that leads to the digitization of the analysis and further improvement of detection limit to only hundreds of molecules per sample. The rapid and noninvasive monitoring of NO in breath using SPs may lead to multifaceted health monitoring assays, which will be easily accessible for many people.

2. Results and Discussion

2.1. Self-Assemblies of SPs

GQDs were prepared by "top-down" oxidation[35] and showed high polydispersity and diameters from 2 to 8 nm (**Figure** 1b). Since the fluorescent properties of GQDs are size-dependent, the low uniformity of GQDs is expected to significantly increase the signal errors in the fluorescence assay.[36] However, self-limited assembly processes can transform polydispersed NPs into nearly monodispersed assemblies.[1] GQDs were observed to assemble in a wide spectrum of morphologies, where the

self-limitation of nanoassemblies manifests in different dimensions.[4] Self-limitation in 1D and 2D leads to nanochains or nanosheets, respectively, with a uniform diameter or thickness 1 or 2 dimensions but not in 3 dimensions (3D). Only limitations enforced on spatial dimensions isotropically will drive the formation of spherical SPs with overall size uniformity.

We assembled GQDs with SOD to complement the biological properties of the protein with the fluorescence and biocompatibility of GQDs. The self-assembly process was induced by the addition of lanthanide ions, in particular Tb^{3+} (**Figure** 2a), forming strong coordination bonds with carboxyl groups at the edges of the graphene sheets. However, triply charged lanthanide ions tend to form branched aggregates (Figure 2a for Tb^{3+} and Figure S3 (Supporting Information) for Y^{3+}, Eu^{3+}, Ce^{3+}, and Gd^{3+}) when added to GQD dispersions because these coordination bonds are rigid and exhibit high spatial anisotropy. Flexible bridges from semiellipsoidal SOD units that partially unfold, dramatically reduce the anisotropy of the coordination assemblies with lanthanide ions and transform branched aggregates into spherical SPs (Figure 1c for Tb^{3+} and Figure S4, Supporting Information for Y^{3+}, Eu^{3+}, Ce^{3+} and Gd^{3+}). First-principle calculations and molecular dynamics (MD) simulations were performed to uncover the mechanisms for shape change from branched aggregates to SPs. Density functional theory (DFT) calculations showed that the optimal geometry for the center-metal-center angle, Φ, for the GQD-Tb^{3+}-GQD assembly was ≈180° leading to the linear assemblies with a C_2 symmetry (Figure S5a, Supporting Information). This geometry of the coordination bridges in the GQD-Tb^{3+}-GQD assembly units forces them to align themselves with respect to each other during the assembly, propagating the symmetry of the individual blocks through all the scales, which can be recognized in their preferential formation of chains. The HOMO and LUMO for GQD-Tb^{3+}-GQD assembly displayed remarkable long-range conjugation between the aromatic systems of GQDs (Figure S5b,c, Supporting Information). The construction of the conjugated structure was due to the mixing of π^* localized molecular orbitals (LMOs) of GQDs and f-LMOs of the Tb^{3+} ion. Electron delocalization is maximized when the GQD-Tb^{3+}-GQD assembly has a linear geometry.

It is known that Tb^{3+} forms coordination bonds to the carboxyl groups of Asp and the Glu residues of proteins.[37] DFT-based calculation showed the Φ for the GQD-Tb^{3+}-Asp assembly was 147.9°, which indicated that the C_2 symmetry was broken (Figure 1g), and no obvious conjugation was displayed in the corresponding HOMO and LUMO (Figure S6, Supporting Information). The flexible peptide chains of SOD further increase the adaptability of the Φ for the GQD-Tb^{3+}-SOD assembly. All-atom MD simulations revealed that the Φ for the GQD-Tb^{3+}-SOD assembly decreased from ≈180 to 63.9° inferring a complete break of C_2 symmetry (Figure 1g). Removal of the preferential bonding axis enables the nanoassembly to maximize short-range attractions, which leads to particles with spherical shapes (Figure 1c,d).

We further investigated the geometry of GQD-Tb^{3+}-SOD assemblies for different SOD content. SPs formed only at the specific weight ratio of GQD:SOD of 60:40. Otherwise, network-shaped aggregates were formed instead of SPs (Figure 2b). A common parameter for the quantitative analysis
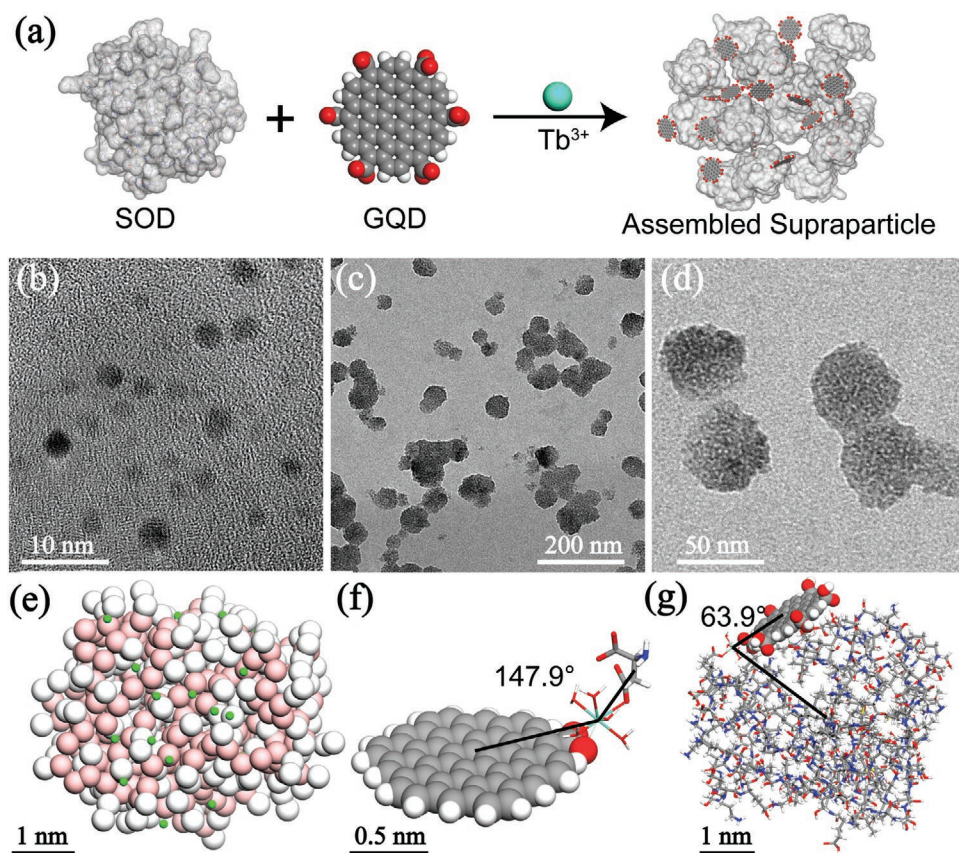
Figure 1. Formation of SPs from GQDs and SOD with terbium ions as metal coordination bridges. a) Schematic illustration of the formation process of SPs. b,c) TEM images for pristine GQDs (b) and SPs (c), and d) high-resolution TEM image for SPs. e) Snapshots of MD simulations for coarse-grained model of Tb^{3+} ions absorbed onto SOD proteins, f) atomistic model for the terbium coordination bridge between a carboxylized GQD and a Glu molecule, and g) atomistic model the angled terbium coordination bridge between a carboxylized GQD and a Glu residue of the SOD.

of these dissimilar assembly patterns is the dimensionless scale index, Γ, (Figure 2d) calculated as a ratio of the largest to the smallest geometric measure of assemblies.[6] When 20% SOD was added, the Γ of the network nanochains significantly dropped from 42.3 to 9.1. At the critical point of 40% SOD, Γ = 2.4, which subsequently increased with a greater concentration of SOD. Irregular aggregates were observed for GQD-Tb^{3+}-SOD assemblies with 60% or more SOD (Figure 2c,d).

2.2. Fluorescence Assay for Nitric Oxide (NO)

It is known that SOD is involved in NO metabolism.[38] Inspired by previous studies of SOD for NO detection,[38–41] we tested NO sensing using GQD-Tb^{3+}-SOD SPs. Nanoscale porosity of SPs, originating from the polydispersity of the constituent GQDs, helps the fast diffusion for small NO molecules to penetrate into these nanoassemblies. We observed that the GQD-Tb^{3+}-SOD SPs did not show strong fluorescence because the light emission of Tb^{3+} is efficiently quenched by Cu (II) ions[42] in SOD. The intensity of the green fluorescence from Tb^{3+} increased, however, 35 times, when NO was present (**Figure 3**a), due to the reduction of Cu (II) to Cu (I) by NO in SOD's reaction center. We further optimized the GQD:SOD ratio to obtain a better analytical performance (Figure 2e).

Coincidently, it was found that the SPs with a 60:40 GQD/SOD ratio containing ≈200 SOD units showed the highest enhancement of Tb^{3+} light emission. Importantly, neither GQD nor SOD alone sensitized Tb^{3+} fluorescence to the degree observed in the SPs, and the close integration of all the components into SPs is required for fluorescence enhancement, which is due to the close range requirements of excited state energy transfer via through-space tunneling (≈2 nm).[43]

2.3. Mechanism for Nitric Oxide Detection

Fluorescent properties of SPs incorporating either SOD with copper ions reduced from Cu (II) to Cu (I) by ascorbic acid or SOD with copper ions extracted by excess EDTA were investigated to understand better the energy transfer processes in self-limited assemblies. Cu-free-SOD showed higher fluorescence intensity than pristine SOD when mixed with 1×10^{-3} м Tb^{3+} solution. In an analogous condition, Cu (I)-SOD showed 8.8 times higher fluorescence intensity than Cu-free-SOD. We concluded that Cu (I) ions sensitize the fluorescence of Tb^{3+} by stimulation of nonradiative intersystem crossing processes, enabling the population of the otherwise symmetry-forbidden radiative state, similar to the optical effects of Ag (I).[44,45] High local concentrations of both Cu (I) and Tb^{3+} in SPs make this sensitization
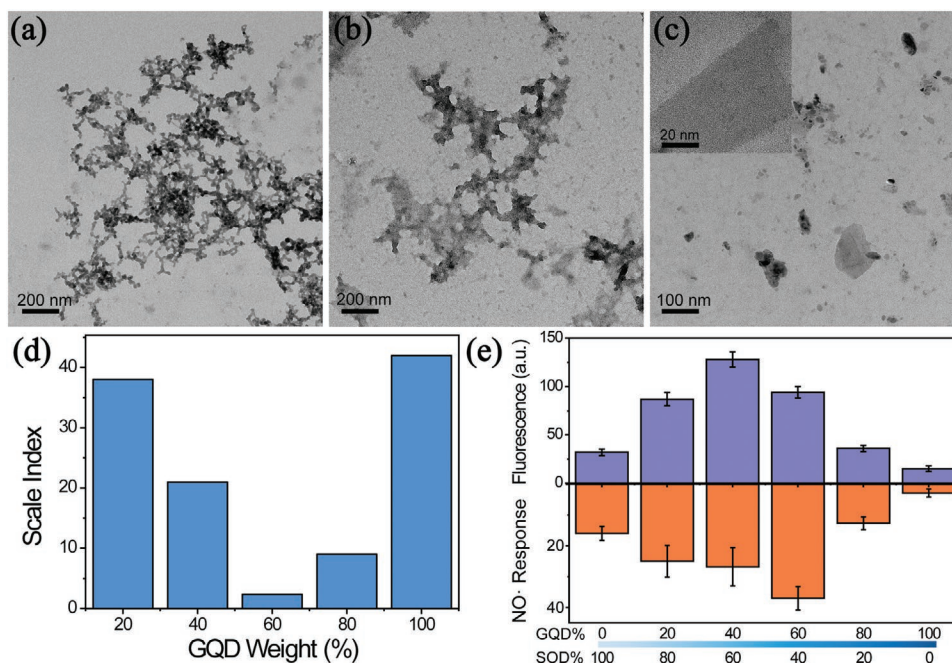
Figure 2. Optimization of the morphology, size dispersity, and fluorescent properties. a–c) TEM images for the coordination nanoassemblies of: a) 1 mg mL^{-1} GQDs, b) 0.8 mg mL^{-1} GQDs, and 0.2 mg mL^{-1} SOD, and c) 0.4 mg mL^{-1} GQDs and 0.6 mg mL^{-1} SOD. d) Size dispersity of the nano-assemblies versus GQD weight percentage in the assemblies. e) Fluorescence intensities and the fluorescence responses to NO versus GQD/SOD weight percentage in the assemblies.

efficient. X-ray photoelectron spectroscopy (XPS) was applied to verify the reduction of copper by NO molecules (Figure S8, Supporting Information). The original Cu (I)–SPs showed a 2p 2/3 peak at 932.6 eV while that in Cu (II)–SPs was positioned at 934.7 eV with satellite peaks between 945 and 940 eV, which is characteristic for Cu (II).[46] Moreover, electron paramagnetic resonance (EPR) spectra for Cu (II)–SPs and Cu (I)–SPs were collected (Figure S9, Supporting Information). It was observed that pristine Cu (II)–SPs showed a pair of strong EPR peaks demonstrating the existence of an unpaired electron in Cu (II). After nitric oxide treatment, the EPR peaks disappeared, corresponding to the XPS result that all the Cu (II) ions were reduced to Cu (I) by NO. DFT calculations of copper ions and their surrounding ligands in SOD (Figure 3c) showed a concomitant structural change after the central Cu (II) was reduced to Cu (I). The Cu (II) reaction site showed a smaller HOMO–LUMO gap of 1.93 eV (calculated from DFT), which acted as effective energy acceptor of Tb^{3+} emission (2.28 eV), and quenched its luminescence (Figure 3d). The DFT-calculated HOMO–LUMO gap for the Cu (I) reaction site was at 4.87 eV (254 nm). This change is essential in the context of the optical properties of SPs because it overlaps with the absorption band of Tb^{3+} at 280 nm and thus permits excitonic energy transfer from reduced SOD to the lanthanide fluorophore. Furthermore, the HOMO–LUMO gap of GQDs used to construct SPs is located at 300 nm (4.13 eV), which also overlaps with the same band of Tb^{3+} (4.40 eV). Therefore, the tight physical proximity of Tb^{3+} to both donors of excitonic energy predisposed SPs for funneling the photonic energy to a single emitter. To some degree, the coupling of different optical and electron transfer effects in SPs is analogous to those observed in nanoscale photosynthetic assemblies in bacteria and plants.

Time-resolved emission decay[37] was measured to further understand the energy transfer pathways in GQD-Tb^{3+}-SOD SPs (Figure S10, Supporting Information). For the copper-free SPs, the fluorescence decay displayed a lifetime of 976 ± 4 µs, which is typical for the symmetry-forbidden emission from Tb^{3+}. The monoexponential decay implies a standard radiative recombination of the excited state and chelation of Tb^{3+} in SPs. The SPs from SOD treated with ascorbic acid showed a similar fluorescence decay profile with a single lifetime of 917 ± 3 µs. Shortening of the lifetime is associated with greater "allowance" of the Tb^{3+} transition due to spin–orbit coupling with Cu (I). In the presence of Cu (II), however, the fluorescence showed a biexponential decay with much shorter lifetimes being consistent with efficient quenching of Tb^{3+} emission by Cu (II). One exponent describes the energy transfer from Tb^{3+} to Cu (II), while the other one corresponds to the characteristic time of energy transfer from GQDs to the Tb^{3+}.

The enhancement of light emission for different NO concentrations (**Figure 4**a) was further studied to determine the limit of detection (LOD) for this biological marker. The LOD in dispersion was calculated to be 10×10^{-12} M. Such a low LOD considerably exceeds the requirements for NO detection, for instance, in brain with expected range of 10×10^{-9} M < [NO] < 1000×10^{-9} M,[47] and in breath with an expected range of 30×10^{-9} M < [NO] < 1500×10^{-9} M (1 ppbv < [NO] < 50 ppbv, where ppbv is parts per billion by volume). SPs showed a 2–3 magnitude order of improvement compared to NO biosensors based on copper complexes.[39]

In a conventional fluorescence assay, one analyte molecule usually causes a fluorescent response by only one probe molecule. Amplification of fluorescence response can be attained by enzymatic catalysis,[48] multiple recognition,[49]
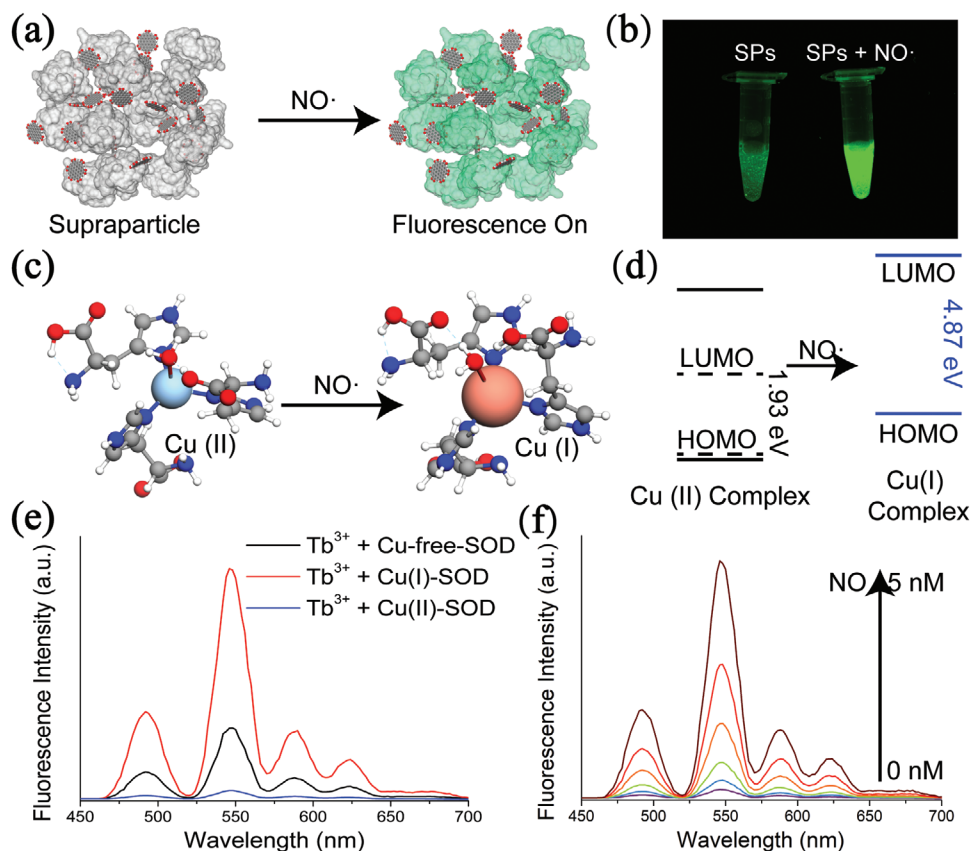
Figure 3. SPs for fluorescent detection of NO and the mechanism illustrations. a) Schematic illustration and b) photograph of the SPs for fluorescent detection of NO. c) DFT optimized structures for the coordination centers of copper (I) and (II) in SOD and d) corresponding molecular orbital energies. e) Fluorescence spectra for terbium ion sensitization by copper-free, copper (I), and copper (II) SODs. f) Fluorescence spectra for SPs in the absence and presence of 50×10^{-12} M, 100×10^{-12} M, 200×10^{-12} M, 1×10^{-9} M, 2×10^{-9} M, 5×10^{-9} M NO, respectively.

and delocalized energy states.[50] Coarse-grained MD simulations showed that there were statistically 29 ± 3 sites in each SP where Tb^{3+} is in close proximity to SOD (Figure 1e). The average distance from Tb^{3+} to the copper center in SOD is approximately 1.9 nm, inferring highly efficient energy transfer between them.[43] That is, the reduction of single Cu (II) ion will lead to the luminescence recovery of multiple Tb^{3+} fluorophores. Stimulation of the forbidden radiative transitions in Tb^{3+} by Cu (I) further enhanced the luminescence.[37] As a result, the sensitivity of SPs to NO was improved by at least two orders of magnitude compared to conventional NO probes.[49]

2.4. Nitric Oxide Detection in Biological Specimens

Being noninvasive, NO breath assays can provide timely information about lung conditions,[51] asthmatic spasms,[31] SARS/COVID-19 infections,[32] and other health problems.[28] Thus, measurements of NO in breath were performed using SP-based fluorescence. Three healthy male volunteers supplied breath samples for analysis (**Table 1**). The average concentration of NO was found to be 9.8 ppbv ($n = 3$, range from less than 4 to 19 ppbv), which is typical for healthy humans.[52,53] The results of the SP-based assays were also consistent with a "gold standard" for NO detection—the method based on 4,5-diaminofluorescein

(DAF-2).[54,55] In addition to the much improved LOD, SP-based assays can also be reusable up to several times; SPs can be reactivated by centrifugation and copper (II) recovery (Figure S12, Supporting Information).

These observations stimulated us to look further into the capabilities of our SPs for NO detection in health monitoring, evaluating its selectivity against reactive oxygen (ROS) and nitrogen (RNS) species. SP-based assays displayed the selective NO fluorescence response with $(F - F_0)/F_0$ in excess of 25 while all the other competing ROS and RNS, including NO_2^-, NO_3^-, HNO, $ONOO^-$, H_2O_2, $\cdot OH$, $^1O_2$, O_2^-, and ClO^-, remained below 5 (Figure 4b).

To understand the sensitivity limits of NO detection with SPs and make a step toward (a) chip-based portable NO detectors and (b) digital read-out of the signal. The transition from traditional analog to advanced digital methods based on counting of single luminescent particles opens the door to a drastic improvement of both reliability and sensitivity of the bioanalysis. Note that it is not possible for single GQDs, proteins, or luminescent due to small size, but it becomes possible for SPs with a diameter of 50 nm and size uniformity provided by a self-limited mechanism of assembly. Also important, that when the particle size becomes too large the digital read-out becomes less effective because the luminescence emission is only limited to the particle surface.

**ADVANCED
SCIENCE NEWS**
www.advancedsciencenews.com

**ADVANCED
MATERIALS**
www.advmat.de
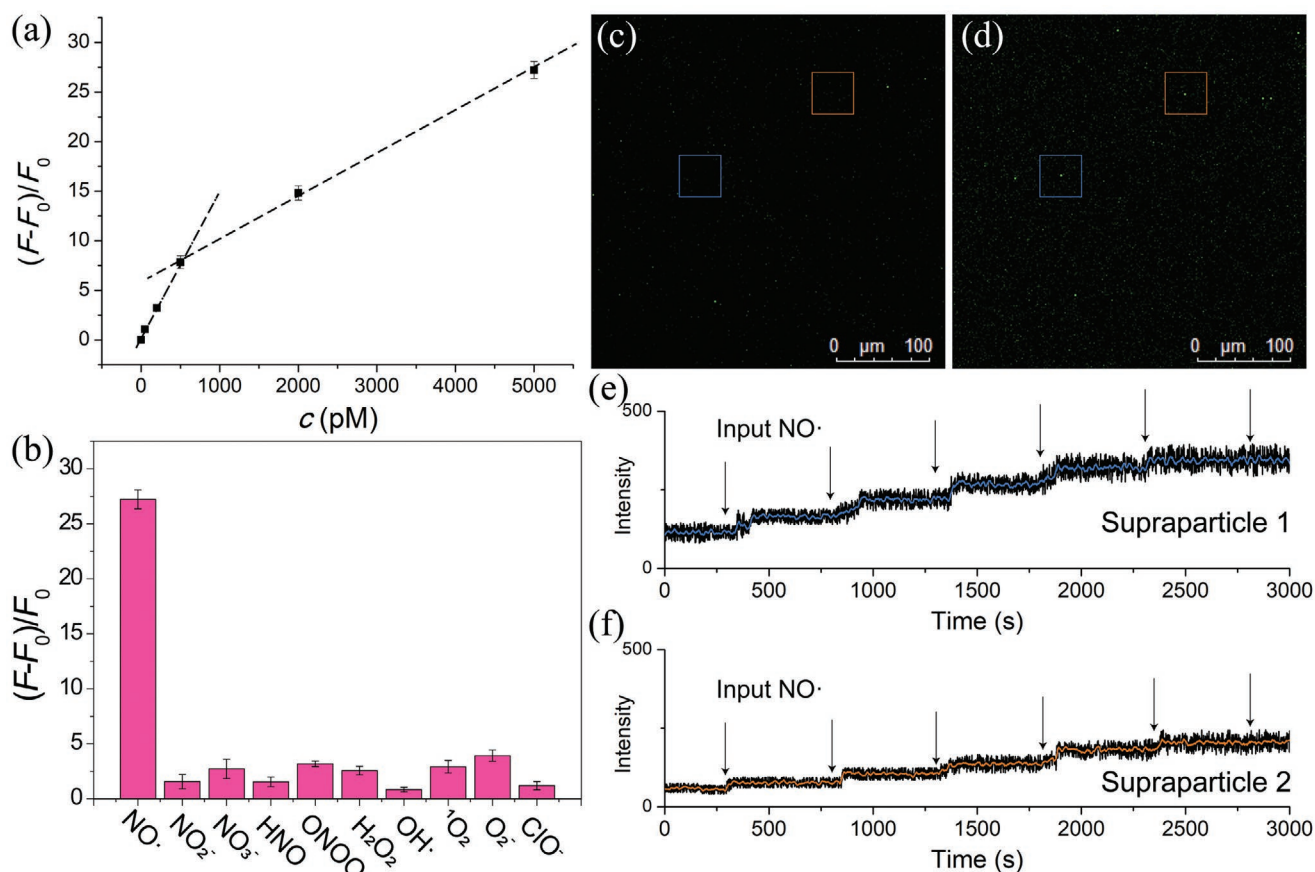
Figure 4. Particle counting format for fluorescence assay for NO detection. a) Linear plot of SPs-based fluorescence assay of NO (a) and b) the corresponding selectivity. c,d) Fluorescence images by confocal microscopy for SPs before (c) and after (d) NO addition. e,f) Fluorescence intensities for two individual SPs with six-step NO inputs (100×10^{-12} M, every 500 s).

To take investigate these possibilities, we spin-coated GQD-Tb^{3+}-SOD SPs on glass, depositing approximately 10^6 SPs per 1×1 cm^2 slide (Figure S13, Supporting Information). To show the broad applicability of the test and the advantages of high sensitivity derived from the SP engineering, we exposed these slides to NO-containing biofluid.[56] Aliquots carrying 100×10^{-12} M (10 μL, 6×10^8 molecules) of NO were injected into a microscale liquid cell with a volume of 1 mL every 500 seconds (Figure 4c,d). We used SP-coated slides, integrated with CCD camera that were themselves integrated with microfluidic devices, to acquire the fluorescence intensities of individual SPs. The ability to read-out responses of single SPs multiple times rather than the single volume of a dispersion represents a considerable advantage of self-limited assemblies over dyes that results in significant enhancement of signal-to-noise ratio due to the large number of SPs in the field of view. The registered signal of single SPs increased stepwise in response to each addition of NO solution to the microfluidic

device (Figure 4e,f), eventually reaching a plateau. This experimental series indicates that using our single-particle detection protocol, one SP gives a distinct optical response to as few as 600 molecules of NO.

3. Conclusions

Self-limited nanoassemblies were engineered from GQDs and SODs by bridging them with lanthanide ions. The proximal position of all the components in the SPs obtained for green-fluorescent Tb^{3+} enabled efficient energy transfer between the nanoscale and ionic subunits, which engendered "turn-on" luminescence detection of NO with record sensitivity being able to detect NO concentrations as low as 10×10^{-12} M. SP assays also enabled transition from analog to digital read-out of the bioanalysis that leads to further improvement of sensitivity making possible identification as few as 600 molecules per 1 mL in dispersion and single-particle assays. Opening a new venue in the utilization of self-limited nanoassemblies, NO detection may lead to a facile detection of several diseases including rapid screening for pulmonary inflammations. High sensitivity, simplicity, and noninvasive nature of SP assays make possible their wide utilization for in-home health monitoring. Implementation of chiroptically active GQDs in

Table 1. Detection of NO concentration in breath (ppbv).

Method	Volunteer 1	Volunteer 2	Volunteer 3
SPs	4.7 ± 1.3	18.2 ± 3.6	6.5 ± 3.2
DAF-2	5.2 ± 2.2	17.1 ± 4.1	7.3 ± 1.2

self-limited nanoassemblies may further expand the spectrum of biological analytes to include chiral small molecules.

Conflict of Interest

The authors declare no conflict of interest.

Data Availability Statement

The data that support the findings of this study are available from the corresponding authors upon reasonable request.

[1] Y. Xia, T. D. T. D. Nguyen, M. Yang, B. Lee, A. Santos, P. Podsiadlo, Z. Tang, S. C. Glotzer, N. A. Kotov, *Nat. Nanotechnol.* **2011**, *6*, 580.

[2] S. Li, J. Liu, N. S. Ramesar, H. Heinz, L. Xu, C. Xu, N. A. Kotov, *Nat. Commun.* **2019**, *10*, 4826.

[3] J. Il Park, T. D. Nguyen, G. de Queirós Silveira, J. H. Bahng, S. Srivastava, G. Zhao, K. Sun, P. Zhang, S. C. Glotzer, N. A. Kotov, *Nat. Commun.* **2014**, *5*, 3593.

[4] Z. Qu, W.-J. Feng, Y. Wang, F. Romanenko, N. A. Kotov, *Angew. Chem.* **2020**, *59*, 8542.

[5] A. Aggeli, I. A. Nyrkova, M. Bell, R. Harding, L. Carrick, T. C. B. McLeish, A. N. Semenov, N. Boden, *Proc. Natl. Acad. Sci. USA* **2001**, *98*, 11857.

[6] W. Jiang, Z. Qu, P. Kumar, D. Vecchio, Y. Wang, Y. Ma, J. H. Bahng, K. Bernardino, W. R. Gomes, F. M. Colombari, A. Lozada-Blanco, M. Veksler, E. Marino, A. Simon, C. Murray, S. R. Muniz, A. F. de Moura, N. A. Kotov, *Science* **2020**, *368*, 642.

[7] J. Yan, W. Feng, J.-Y. Kim, J. Lu, P. Kumar, Z. Mu, X. Wu, X. Mao, N. A. Kotov, N. A. Kotov, N. A. Kotov, *Chem. Mater.* **2020**, *32*, 476.

[8] E. Piccinini, D. Pallarola, F. Battaglini, O. Azzaroni, *Mol. Syst. Des. Eng.* **2016**, *1*, 155.

[9] K. Zhang, J. Yi, D. Chen, *J. Mater. Chem. A* **2013**, *1*, 14649.

[10] K. Niikura, N. Iyo, Y. Matsuo, H. Mitomo, K. Ijiro, *ACS Appl. Mater. Interfaces* **2013**, *5*, 3900.

[11] S. Jiang, M. Chekini, Z. B. Qu, Y. Wang, A. Yeltik, Y. Liu, A. Kotlyar, T. Zhang, B. Li, H. V. Demir, N. A. Kotov, *J. Am. Chem. Soc.* **2017**, *139*, 13701.

[12] W. Yan, L. Xu, C. Xu, W. Ma, H. Kuang, L. Wang, N. A. Kotov, *J. Am. Chem. Soc.* **2012**, *134*, 15114.

[13] K. Zhu, D. Wang, J. Liu, *Nano Res.* **2009**, *2*, 1.

[14] S. Liu, T. H. Zeng, M. Hofmann, E. Burcombe, J. Wei, R. Jiang, J. Kong, Y. Chen, *ACS Nano* **2016**, *5*, 6971.

[15] C. Xia, S. Zhu, T. Feng, M. Yang, B. Yang, *Adv. Sci.* **2019**, *6*, 1901316.

[16] D. Pan, J. Zhang, Z. Li, M. Wu, *Adv. Mater.* **2010**, *22*, 734.

[17] L. A. Ponomarenko, F. Schedin, M. I. Katsnelson, R. Yang, E. W. Hill, K. S. Novoselov, A. K. Geim, *Science* **2008**, *320*, 356.

[18] H. Sun, L. Wu, W. Wei, X. Qu, *Mater. Today* **2013**, *16*, 433.

[19] X. Yan, X. Cui, L.-S. Li, *J. Am. Chem. Soc.* **2010**, *132*, 5944.

[20] K. Li, W. Liu, Y. Ni, D. Li, D. Lin, Z. Su, G. Wei, *J. Mater. Chem. B* **2017**, *5*, 4811.

[21] J. Shen, Y. Zhu, X. Yang, C. Li, *Chem. Commun.* **2012**, *48*, 3686.

[22] R. Ye, C. Xiang, J. Lin, Z. Peng, K. Huang, Z. Yan, N. P. Cook, E. L. G. Samuel, C.-C. Hwang, G. Ruan, G. Ceriotti, A.-R. O. Raji, A. A. Martí, J. M. Tour, *Nat. Commun.* **2013**, *4*, 2943.

[23] Q. Zhang, X. Wang, Y. Zhu, *J. Mater. Chem.* **2011**, *21*, 12132.

[24] Y. Ma, K. Promthaveepong, N. Li, *ACS Appl. Mater. Interfaces* **2017**, *9*, 10530.

[25] H. Cheng, Y. Zhao, Y. Fan, X. Xie, L. Qu, G. Shi, *ACS Nano* **2012**, *6*, 2237.

[26] H. Cheng, L. Wang, M. Mollica, A. T. Re, S. Wu, L. Zuo, *Cancer Lett.* **2014**, *353*, 1.

[27] K. M. Sanders, S. M. Ward, *Am. J. Physiol. Gastrointest. Liver Physiol.* **1992**, *262*, G379.

[28] X. Chen, F. Niroomand, Z. Liu, A. Zankl, H. A. Katus, L. Jahn, C. P. Tiefenbacher, *Basic Res. Cardiol.* **2006**, *101*, 346.

[29] T. Malinski, *J. Alzheimer's Dis.* **2007**, *11*, 207.

[30] N. Pitsikas, *Nitric Oxide* **2018**, *77*, 6.

[31] M. Belvisi, P. J. Barnes, S. Larkin, M. Yacoub, S. Tadjkarimi, T. J. Williams, J. A. Mitchell, *Eur. J. Pharmacol.* **1995**, *283*, 255.

[32] S. Åkerström, M. Mousavi-Jazi, J. Klingström, M. Leijon, Å. Lundkvist, A. Mirazimi, *J. Virol.* **2005**, *79*, 1966.

[33] E. Keyaerts, L. Vijgen, L. Chen, P. Maes, G. Hedenstierna, M. Van Ranst, *Int. J. Infect. Dis.* **2004**, *8*, 223.

[34] P. Mehta, D. F. McAuley, M. Brown, E. Sanchez, R. S. Tattersall, J. J. Manson, *Lancet* **2020**, *395*, 1033.

[35] Z. Qu, M. Zhang, T. Zhou, G. Shi, *Chem. - Eur. J.* **2014**, *20*, 13777.

[36] J. Peng, W. Gao, B. K. Gupta, Z. Liu, R. Romero-Aburto, L. Ge, L. Song, L. B. Alemany, X. Zhan, G. Gao, S. A. Vithayathil, B. A. Kaipparettu, A. A. Marti, T. Hayashi, J.-J. Zhu, P. M. Ajayan, *Nano Lett.* **2012**, *12*, 844.

[37] Z.-Y. Lin, Z. Qu, Z.-H. Chen, X.-Y. Han, L.-X. Deng, Q. Luo, Z. Jin, G. Shi, M. Zhang, *Anal. Chem.* **2019**, *91*, 11170.

[38] M. E. Murphy, H. Sies, *Proc. Natl. Acad. Sci. USA* **1991**, *88*, 10860.

[39] M. H. Lim, B. A. Wong, W. H. Pitcock, D. Mokshagundam, M.-H. Baik, S. J. Lippard, *J. Am. Chem. Soc.* **2006**, *128*, 14364.

[40] D. J. Lamb, M. L. Tickner, S. M. O. Hourani, G. A. A. Ferns, *Int. J. Exp. Pathol.* **2005**, *86*, 247.

[41] A. G. Estévez, J. P. Crow, J. B. Sampson, C. Reiter, Y. Zhuang, G. J. Richardson, M. M. Tarpey, L. Barbeito, J. S. Beckman, *Science* **1999**, *286*, 2498.

[42] S.-F. Xue, L.-F. Lu, Q.-X. Wang, S. Zhang, M. Zhang, G. Shi, *Talanta* **2016**, *158*, 208.

[43] K. Redeckas, V. Voiciuk, D. Zigmantas, R. G. Hiller, M. Vengris, *Biochim. Biophys. Acta, Bioenerg.* **2017**, *1858*, 297.

[44] M. Zhang, Z. B. Qu, H. Y. Ma, T. Zhou, G. Shi, *Chem. Commun.* **2014**, *50*, 4677.

[45] M. Isaac, S. A. Denisov, A. Roux, D. Imbert, G. Jonusauskas, N. D. McClenaghan, O. Sénèque, *Angew. Chem., Int. Ed.* **2015**, *54*, 11453.

[46] M. A. Salim, G. D. Khattak, N. Tabet, L. E. Wenger, *J. Electron Spectrosc. Relat. Phenom.* **2003**, *128*, 75.

[47] T. Malinski, F. Bailey, Z. G. Zhang, M. Chopp, *J. Cereb. Blood Flow Metab.* **1993**, *13*, 355.

[48] N. Xia, L. Liu, M. G. Harrington, J. Wang, F. Zhou, *Anal. Chem.* **2010**, *82*, 10151.

[49] K. Soga, K. Tokuzen, K. Tsuji, T. Yamano, H. Hyodo, H. Kishimoto, *Eur. J. Inorg. Chem.* **2010**, *2010*, 2673.

[50] S. W. Thomas, G. D. Joly, T. M. Swager, *Chem. Rev.* **2007**, *107*, 1339.

[51] Y. Zou, X. Zhang, C. An, C. Ran, K. Ying, P. Wang, *Biomed. Microdevices* **2014**, *16*, 927.

[52] J. K. Robinson, M. J. Bollinger, J. W. Birks, *Anal. Chem.* **1999**, *71*, 5131.

[53] A. M. Leone, L. E. Gustafsson, P. L. Francis, M. G. Persson, N. P. Wiklund, S. Moncada, *Biochem. Biophys. Res. Commun.* **1994**, *201*, 883.

[54] H. Kojima, N. Nakatsubo, K. Kikuchi, S. Kawahara, Y. Kirino, H. Nagoshi, Y. Hirata, T. Nagano, *Anal. Chem.* **1998**, *70*, 2446.

[55] E. Planchet, W. M. Kaiser, *J. Exp. Bot.* **2006**, *57*, 3043.

[56] Z. Qu, X. Zhou, L. Gu, R. Lan, D. Sun, D. Yu, G. Shi, *Chem. Commun.* **2013**, *49*, 9830.